

Short-circuit current density mapping for solar cells

M. Padilla*, B. Michl, B. Thaidigsmann, W. Warta, M.C. Schubert

Fraunhofer ISE, Fraunhofer Institute for Solar Energy Systems, Heidenhofstr. 2, 79110 Freiburg, Germany



ARTICLE INFO

Article history:

Received 22 July 2013

Received in revised form

12 September 2013

Accepted 13 September 2013

Available online 9 October 2013

Keywords:

Silicon
Solar cell

Current density
Loss-analysis
Mapping
Cast-mono

ABSTRACT

A map of local short-circuit current density (J_{SC}) of a solar cell at standard irradiance spectra is a desirable source of information for current-loss analysis and device optimization. In this work, we present a new and easily implementable method to obtain such J_{SC} maps as well as local external quantum efficiency graphs with a spatial resolution of about 100 μm, exemplified for silicon solar cells. The method is based on a pixel by pixel interpolation of external quantum efficiency maps obtained by spectrally resolved light-beam induced current measurements (SR-LBIC). The local data is integrated with an AM1.5G spectrum to obtain a J_{SC} map with no additional measurement time beyond SR-LBIC image acquisition. The averaged currents over a map are in good agreement with global current–voltage measurements. Some of the possible applications of this method are presented and exemplified, including local quantum efficiency of a cast-mono solar cell, separation of J_{SC} contributions from front side and bulk, quantitative determination of the electrical shading effect in IBC cells, the impact of the irradiance spectrum on local J_{SC} for indoor photovoltaic applications and also the separation of optical and electrical current losses with newly introduced Pseudo- J_{SC} maps based on internal quantum efficiency maps. Finally, the resulting J_{SC} maps also present valuable information for several existing local cell-parameter imaging methods. This basic approach leads to an easily accessible, spatially resolved short-circuit current loss-analysis, which is in principle applicable to any solar cell structure.

© 2013 Elsevier B.V. All rights reserved.

1. Introduction

The short-circuit current density (J_{SC}) of a photovoltaic device is an essential parameter to characterize its power conversion efficiency. Short-circuit currents densities are often not homogeneous across a device, for example due to regions of low charge carrier lifetimes, locally increased surface recombination, distances to the metal contacts as well as optical heterogeneities in the production process. As industrial silicon solar cells are breaching 20% efficiency, the demand for local optimization of current extraction becomes more crucial.

In this work, we present a new data evaluation method using multiple SR-LBIC measurements obtained from a commercially available measurement setup to calculate short-circuit current density maps. The method is based on a pixel by pixel interpolation of external quantum efficiency (EQE). The result is then spectrally integrated with the AM1.5G (or any arbitrary) spectrum to obtain J_{SC} at each pixel, without the need for scaling with the average globally measured J_{SC} . The main advantage of this technique is that it combines the advantages of spectrally resolved data from local EQE with the figure of merit J_{SC} , which is now accessible

with a high spatial resolution. A J_{SC} map at AM1.5G spectrum is very helpful because it shows the impact on the final short-circuit current density output after all local electrical and optical losses in a finished solar cell.

Measurements of spatially resolved electric currents for the study of photovoltaic devices were introduced in the 1980s. The main research efforts dealt with the assessment of crystallization quality, homogeneity and the microscopic characterization of grain boundaries and diffusion lengths [1–4]. Currents were induced by either a focused electron-beam (EBIC) or light-beam (LBIC). Using LBIC at specific wavelengths was denoted spectrally resolved light-beam induced current (SR-LBIC), which was also employed for the characterization of grain boundaries [4]. SR-LBIC was later used also for large device areas to obtain maps of local quantum efficiency for individual wavelengths and for diffusion length mapping [5–7].

To obtain an SR-LBIC map, a solar cell is held at short-circuit while a light spot at a given wavelength with a diameter between few and several hundred microns scans the surface of the cell and measures the extracted photocurrent. The current is scaled to show EQE, which is the fraction of incident photons that successfully lead to the extraction of an excess carrier from the cell. This efficiency is wavelength dependent, as it can be influenced by the penetration depth in the cell. Nowadays commercially available SR-LBIC systems for solar cell analysis are based on the experiment

* Corresponding author. Tel.: +49 761 4588 5263; fax: +49 761 4588 9250.
E-mail address: milan.padilla@ise.fraunhofer.de (M. Padilla).

by Warta et al. [7]. In Warta's system, multiple modulated laser light sources at distinct wavelengths run simultaneously at different harmonics. Therefore, measurement time is virtually independent of the number of used wavelengths, as long as the frequencies of laser intensity modulations are low enough for typical response times of a solar cell. The signal is demodulated to obtain separate images for each wavelength. SR-LBIC maps are commonly used to determine local diffusion lengths, particularly for multicrystalline silicon solar cells [8,9]. Additionally, the spectrally resolved reflectance (R) can be measured via a photodiode over the sample. Therefore, also internal quantum efficiency maps (IQE) are obtained, which present the ratio of actually absorbed photons to extracted carriers. Thus, IQE maps are free of non-absorption losses. The scaling for EQE and R for a given SR-LBIC setup is commonly performed via the quantum efficiency of a calibrated reference cell, respectively a white-standard. More refined scaling procedures specific to each sample are possible but usually not necessary.

2. Experimental setup and interpolation method

The experimental data for this work was acquired from SR-LBIC measurements from the commercially available LOANA solar cell analysis system by pv-tools GmbH [10]. Modulated laser light was used from six diode-lasers at 405 nm, 532 nm, 670 nm, 780 nm, 940 nm and 1064 nm, all coupled onto the solar cell through an optical fiber. At the focus height used in this work, the FWHM of the Gaussian laser profiles varied for each wavelength and ranged between 100 μm (for 670 nm) and 220 μm (for 405 nm). For size of the investigated structures, the beam-profile had no major effect on the final image, which will be shown in Fig. 5. No bias-light was used in this work, as all samples were assumed to have a linear dependence of current over intensity, which means that injection dependent lifetime effects are neglected. In case of significantly non-linear samples, a bias-light is needed to reduce measurement errors [11]. Such non-linearities and injection dependencies are often observed with dielectric passivation concepts [12]. This non-linearity can strongly impact cells with large area fractions of dielectric passivation (e.g. PERL cells). Intensity variations of the light sources are cancelled out using a monitor detector. The solar cell is kept at 25 °C by a temperature controlled measurement chuck. As shown in Eq. (1), the measured current I_{SC} at a wavelength λ_i and position xy is scaled by the reference $\text{EQE}_{\lambda_i}^{\text{Ref}}$ and reference $I_{\text{SC}}^{\text{Ref}}$ for the particular SR-LBIC setup.

$$\text{EQE}_{\lambda_i}^{xy} = \frac{\text{EQE}_{\lambda_i}^{\text{Ref}}}{I_{\text{SC}}^{\text{Ref}}} I_{\text{SC}}^{xy} \quad (1)$$

The short-circuit current density J_{SC} at a given incident spectral photon flux density $\phi(\lambda)$ is correlated with the $\text{EQE}(\lambda_i)$ via

$$J_{\text{SC}}^{xy} = q \int_{\lambda_1}^{\lambda_2} \text{EQE}^{xy}(\lambda) \phi(\lambda) d\lambda \quad (2)$$

No additional weighting with the pixel and illumination area is necessary, because $\text{EQE}^{xy}(\lambda)$ is not area related. To reduce uncertainties in the local EQE, the step size of the mapping is chosen to be smaller than the laser spot sizes. This makes sure that every part of the cell is illuminated at some point during the measurement. According to Eq. (2), calculating J_{SC}^{xy} requires the function $\text{EQE}^{xy}(\lambda)$ at each pixel. The experimental data from our setup yields $\text{EQE}_{\lambda_i}^{xy}$ for six wavelengths between 405 nm and 1064 nm. This already covers most of the spectral range where the AM1.5G spectrum has significant contributions in silicon. The function $\text{EQE}^{xy}(\lambda)$ is obtained by linear interpolation between the six points known from the SR-LBIC measurements. However, typical silicon

solar cells under AM1.5G spectrum receive contributions to J_{SC} from wavelengths between about 300 nm and 1200 nm, which are beyond the 405–1064 nm range of our SR-LBIC setup. To account for this, we created artificial SR-LBIC images at 300 nm and at 1170 nm by scaling the images at 405 nm and 1064 nm with the ratio between the global EQE at 405 nm and 300 nm, respectively 1064 nm and 1170 nm. Because of a penetration depth of only some tens of nanometers at 405 nm wavelength and few nanometers at 300 nm wavelength, this approximation will not decrease the lateral spatial resolution. This also assumes that the relative lateral differences in local EQE are the same for 300 nm than for 405 nm. At the other end, an actual SR-LBIC measured image at 1170 nm would be more blurred than the 1064 nm image due to a significantly higher penetration depth d in silicon and thus increased scattering of light at the rear side of the cell ($d_{\text{Si}}|_{1064 \text{ nm}} \approx 0.1 \text{ cm}$, $d_{\text{Si}}|_{1170 \text{ nm}} \approx 4.5 \text{ cm}$) [13].

In principle, the interpolation could be refined with physical models and functions but simple linear interpolation has shown sufficiently good results for all silicon solar cells tested for this work and is thus recommendable because it requires less computation time and user input for each sample. Eq. (2) can of course alternatively be applied with spectral response instead of EQE and light intensity instead of photon flux.

Fig. 1 shows the conventionally measured EQE by a monochromator (black line), which was averaged over the whole cell, the average of the linearly interpolated EQE (dashed red line), the average EQE from SR-LBIC measurements (red diamonds) as well as the two additionally inserted interpolation points (white diamonds) from the artificial SR-LBIC images at 300 nm and 1170 nm. The data was obtained from a 15.6 cm × 15.6 cm industrial multicrystalline silicon solar cell. The deviations between the linear interpolation and global measurement can be calculated from their ratio for each wavelength. The average in this example is below 1% and has a standard deviation of 8%, which represents the spread. Such a basic statistical analysis shows how well the SR-LBIC interpolation matches the direct EQE measurement and thus helps estimating the errors of the proposed method for each cell.

Fig. 2 shows the obtained short-circuit current density map of the same cell used for Fig. 1. The average J_{SC} over this map is 33.9 mA cm⁻², while J_{SC} from a traditional sun simulator measurement with a xenon lamp spectrum was 33.3 mA cm⁻². The deviation of about 0.6 mA cm⁻² is of the order of typical estimated errors in non-calibrated IV measurements, which was estimated to be about +/-2% for this sun simulator.

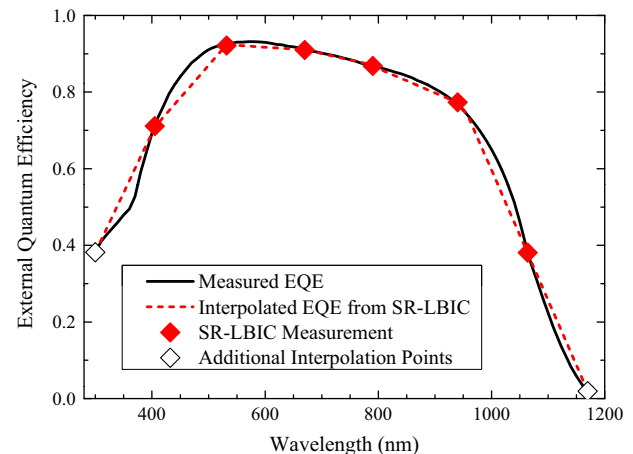


Fig. 1. Averaged, linearly interpolated EQE of a whole industrial silicon solar cell compared to the conventionally measured global EQE. (For interpretation of the references to color in this figure legend, the reader is referred to the web version of this article.)

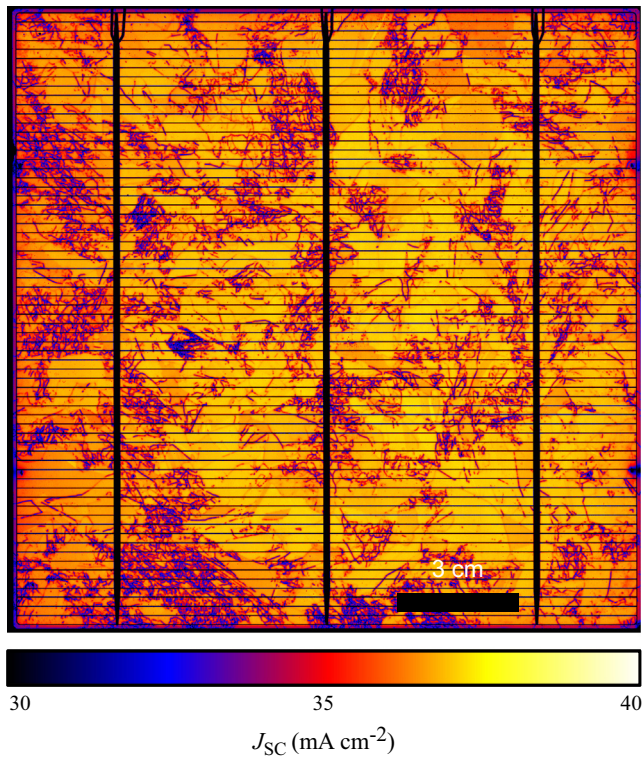


Fig. 2. J_{SC} map of an industrial multicrystalline silicon solar cell.

Data acquisition time with the LOANA SR-LBIC system depends on the step size of each measurement point. At 100 μm step size a measurement time of about two minutes per cm^2 sample surface is required. The interpolation algorithm was implemented in Matlab and requires few minutes computation time on a modern office computer, depending on the sample size.

3. Application examples

3.1. Material quality and local production inhomogeneity of cast-mono solar cells

The presented method allows direct evaluation of the impact of material quality and local device properties for current extraction under AM1.5G spectrum. The following example shows that a local J_{SC} analysis in combination with local EQE can be a fast method of studying the impact of local current losses. Also, it can be used to separate different J_{SC} loss mechanisms all while assessing their impact on the final J_{SC} .

Fig. 3(a) depicts a J_{SC} map of a 15.6 cm × 15.6 cm, alkaline-textured, high-performance metal wrap through (HIP-MWT) silicon solar cell created from p-type cast-mono base material [14]. The averaged J_{SC} over the image is 36.6 mA cm⁻², which is in very good agreement with the 36.9 mA cm⁻² measured by an industrial solar cell tester. Fig. 3(b) shows the interpolated EQE graphs of the regions highlighted in the dashed rectangles in(a).

Region of interest A (Roi A) shows the EQE characteristic and thus J_{SC} observed over most of the bulk of the cell with an average J_{SC} of 38.0 mA cm⁻². In comparison, Roi B is a region with an orientation different from (100) and a high density of dislocations, where defects greatly deteriorate the EQE at wavelengths above 800 nm. The non-(100) crystal orientation of this region made the alkaline-texturing ineffective, which leads to a higher reflectance and ultimately poorer EQE, particularly in the UV regime. This increased reflectance is confirmed by visual inspection as well as

reflectance maps (data not shown). Roi C belongs to a region of the cell edge, with a J_{SC} of 39.8 mA cm⁻², which is almost 2 mA cm⁻² higher than that of Roi A. The reason for this improved performance at the edge of the cell is not fully understood to date. The most probable explanation is an interaction between parasitic deposition of the ARC at the rear and the local contact formation by LFC (laser fired contacts [15]), leading to reduced rear recombination at the edge as an unexpected positive effect. Finally, Roi D, also taken at the edge of the cell, shows a similar enhanced spectral response in the infrared regime, but also shows a lower blue response similar to Roi B caused by the reflectance of the grain structure.

Furthermore, it is possible to quantify the share of J_{SC} contribution between short and long wavelengths, thus separating front and bulk contribution. An example for this is shown in Fig. 3(c) and (d) by integrating J_{SC} between 300 nm and 670 nm, respectively 671 nm and 1170 nm. With this approach, even irregularities in the emitter quality can be measured and quantified in terms of impact on J_{SC} . All of these analyses can conveniently be performed anywhere on the cell with data from a single SR-LBIC measurement.

3.2. Separation of optical and electrical current losses with pseudo- J_{SC} maps

Several commercially available SR-LBIC measurement setups like the one by pv-tools GmbH include parallel acquisition of local current and reflectance data. The interest of internal quantum efficiency is to discern between electrical and optical losses, since the IQE represents the quantum efficiency of the solar cell regarding only photons that actually generated excess charge carriers. Such information can be valuable, especially when there are optical heterogeneities. Thereby, local internal quantum efficiency maps can be calculated as

$$\text{IQE}^{xy}(\lambda) = \frac{\text{EQE}^{xy}(\lambda)}{1 - R^{xy}(\lambda)} \quad (3)$$

Such IQE maps can now be used to interpolate the short-circuit current density in analogy to Eq. 2. We named these resulting new short-circuit current density maps “Pseudo- J_{SC} maps”. The following example shows an extreme case, where optical irregularities strikingly impact the J_{SC} performance. Fig. 4(a) shows a Pseudo- J_{SC} map (top) and a regular J_{SC} map (bottom) of a monocrystalline silicon solar cell that received a non-perfect honeycomb texture via nanoimprint lithography for enhanced absorption in the silicon bulk [16], instead of conventional pyramid texture. In this early attempt of the process development, the honeycomb texturing failed to be imprinted at the sides of cell, leading to a locally planar surface and hence a strongly decreased J_{SC} of ~31 mA cm⁻² as opposed to ~37 mA cm⁻² at the center of the cell.

The Pseudo- J_{SC} map confirms that the losses on the sides are primarily optical losses, as the Pseudo- J_{SC} is mostly homogeneous. Also, this analysis shows the local electrically possible J_{SC} of the device, if all optical losses are eliminated, which is about 39.5 mA cm⁻² in this particular example. In some cases J_{SC} can be decreased by a combination of local optical and electrical properties, such as a poorer SiO₂ passivation at a (111) surface due to higher defect densities [17]. It should be possible to identify such effects with the presented Pseudo- J_{SC} method.

3.3. Local electrical-shading loss of IBC cells and impact of laser beam profile

Interdigitated back contact (IBC) silicon solar cells have all p-n junctions as well as the entire metallization in an interdigitated grid on the backside of the cell, cancelling out optical shading

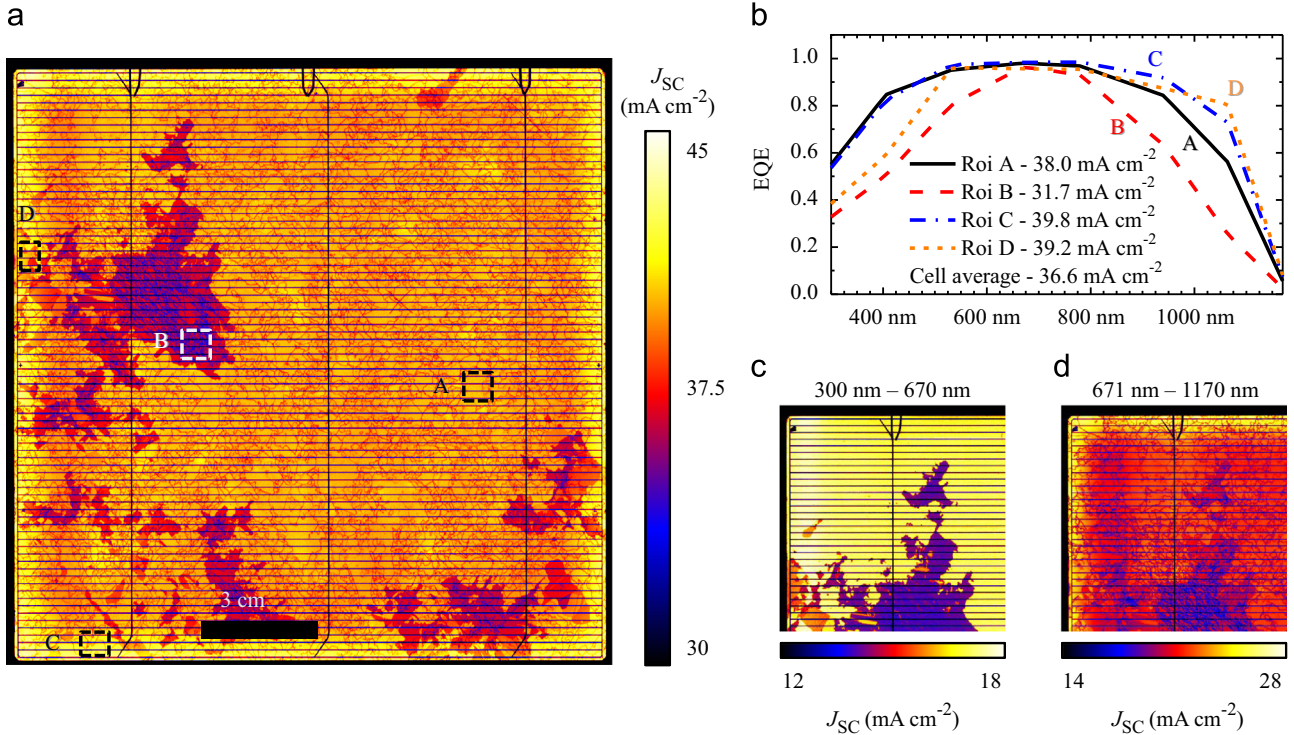


Fig. 3. (a) J_{SC} map of a cast-mono HIP-MWT cell; (b) local EQE graphs of regions highlighted in (a), (c) contribution to J_{SC} between 300 nm and 670 nm, and (d) between 671 nm and 1170 nm.

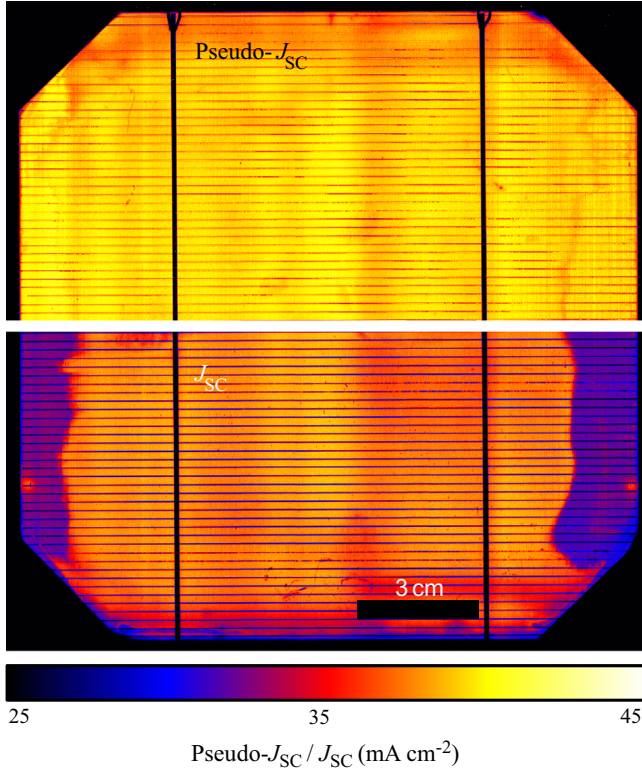


Fig. 4. (a) Pseudo- J_{SC} map (top) obtained from interpolated IQE maps and (b) J_{SC} map obtained from regular EQE maps of a solar cell with an inhomogeneous honeycomb surface texture.

losses and thus allowing conversion efficiencies above 23% in industrial production [18].

The collection efficiency of these cells can be locally decreased by recombination at the back-surface-field region (BSF) and/or an

insufficiently bulk lifetime for minorities that were generated over the BSF to reach the emitter. This well-known effect is often denominated “electrical-shading” and has been studied over EQE by SR-LBIC at single wavelengths [19] and recently also by photoluminescence [20]. The presented method of J_{SC} -mapping now allows direct access to the effective local short-circuit current density loss caused by electrical-shading.

Fig. 5(a) shows the J_{SC} map of an n-type IBC cell, as well as a schematic of the doping structure (bottom). The bright areas at the emitter yield current densities of up to 41.2 mA cm^{-2} while the extracted current densities over the center of the BSF lines drop down to about 33 mA cm^{-2} . **Fig. 5(b)** depicts an averaged line scan over the area in the dashed rectangle in (a), where a baseline of the maximum measured J_{SC} at the center of the emitter (41.2 mA cm^{-2}) was subtracted. The result shows how much J_{SC} is exactly being lost due to the electrical-shading effect at each position. The maximum local loss was found to be 8.0 mA cm^{-2} , while the integral loss over the whole area is 1.7 mA cm^{-2} .

In the examples shown so far, the impact of the beam profile of the SR-LBIC lasers has not been taken into consideration. However, the beam profile can play a role if the desired resolution of the structures is of the order of the FWHM of the laser beams. This is the case for this IBC cell, where the gap between emitter and BSF is only $150 \mu\text{m}$ wide. The laser beam width was determined by a knife-edge measurement, where the reflectance of each laser was measured across the edge of a razor blade. The differentiated signal directly yields the laser profiles, which can be fit well by Gaussian functions (data not shown). These profiles were used to create point-spread-functions to deconvolute the experimental SR-LBIC maps. The two-dimensional deconvolution was performed with the freely available plugin DeconvolutionLab for ImageJ [21,22]. The dashed line in **Fig. 5(b)** shows the J_{SC} loss according to the original SR-LBIC maps and the red line presents the J_{SC} loss after deconvolution of each of the SR-LBIC input maps. As expected, the deconvolution increased the peak loss by about 0.2 mA cm^{-2} and the curve became slightly slimmer. However, the

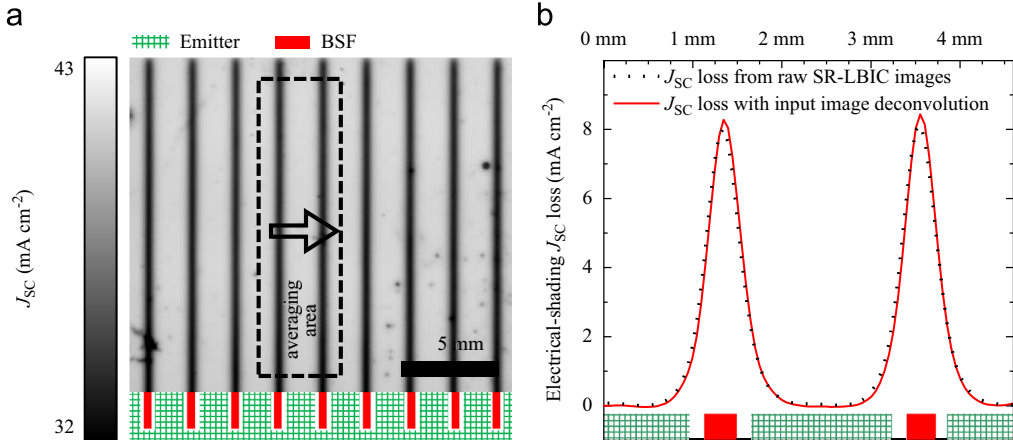


Fig. 5. (a) J_{SC} map of an IBC silicon solar cell and (b) J_{SC} loss by electrical shading across the area highlighted in (a). (For interpretation of the references to color in this figure legend, the reader is referred to the web version of this article.)

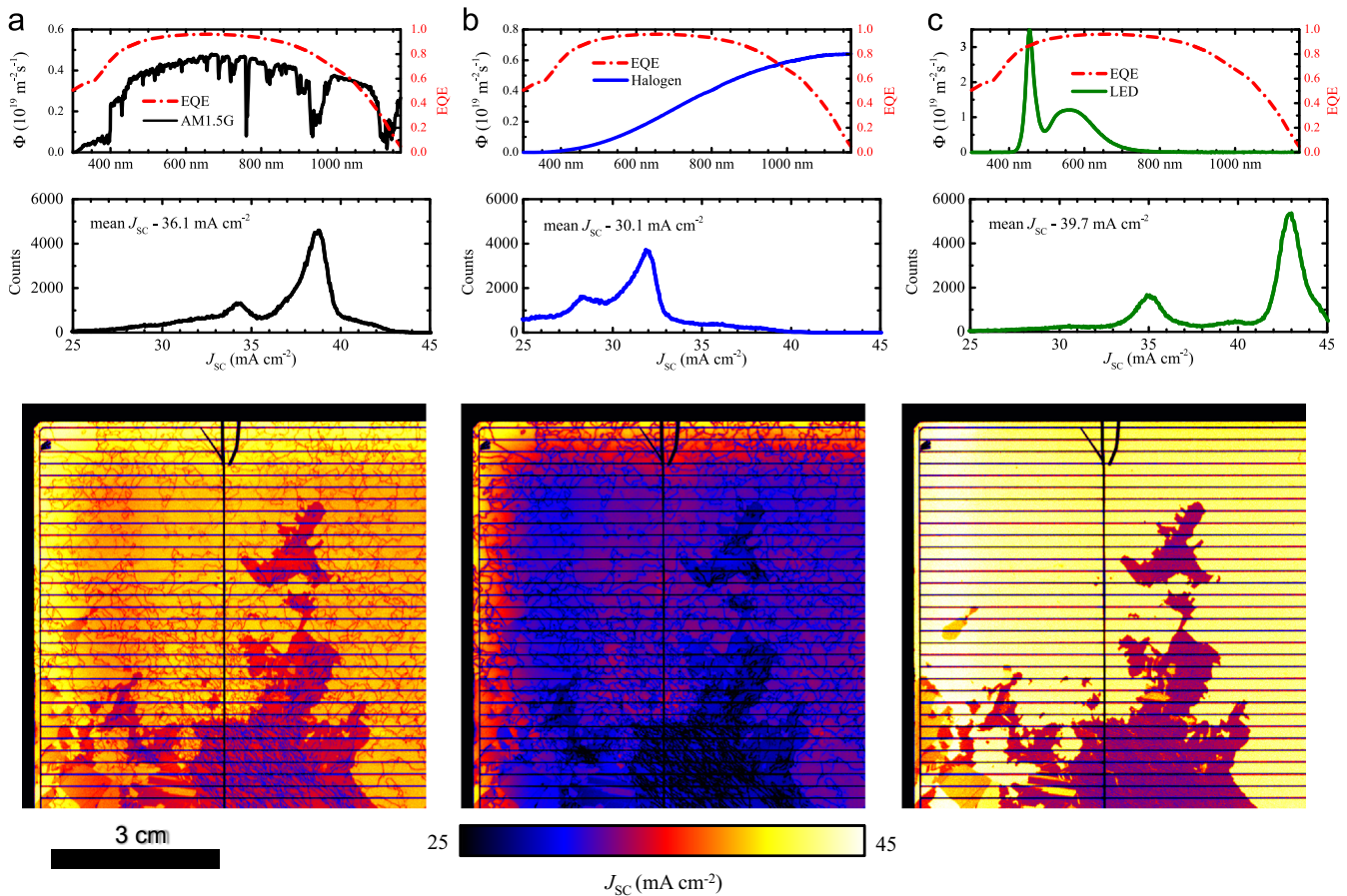


Fig. 6. J_{SC} maps and their histograms of an MWT silicon solar cell at different irradiance spectra with the same integrated photon flux. (a) AM1.5G, (b) sample halogen lamp and (c) sample LED.

effect has no significant impact on the quantitative result and thus no deconvolution is required for this structure size in our particular setup.

3.4. Impact of irradiance spectra for indoor photovoltaics

As stated earlier, the choice of photon-flux for the calculation of a J_{SC} map according to Eq. 2 is arbitrary. Therefore, the presented method can be used to predict the effect on J_{SC} caused by different irradiance spectra. This is particularly of interest for research on

indoor photovoltaics, where the irradiance spectra often strongly deviate from AM1.5G [23,24].

As an example, a 6×6 cm 2 selection of the cast-mono MWT cell shown in Fig. 3 was chosen. Fig. 6 depicts the spectral photon-flux (solid line) and averaged global EQE (dashed line) (top), J_{SC} histogram (middle) and J_{SC} map (bottom) using the AM1.5G spectrum (a), the spectrum of a halogen lamp (b) and the spectrum of a sample Liquiled LED (c). The integrated photon flux between 300 nm and 1170 nm was set to be identical with the AM1.5G flux. The halogen spectrum contains mostly infrared

Table 1

Summary of average J_{SC} obtained by the presented method compared to values from sun simulator measurements.

Cell type	Size type	Av. J_{SC} -LBIC (mA cm ⁻²)	J_{SC} -IV (mA cm ⁻²)	Delta J_{SC} LBIC-IV (mA cm ⁻²)	J_{SC} Deviation (%)	Shown in
1. mc-Si Industrial, Al-BSF	15.6 × 15.6 cm ² , p-type	33.9	33.3	+0.6	+1.8	Figs. 1 and 2
2. mc-Si Industrial, Al-BSF	12.5 × 12.5 cm ² , p-type	35.1	34.7	+0.4	+1.1	Not shown
3. Cast-mono Industrial, Al-BSF	15.6 × 15.6 cm ² , p-type	32.8	33.5	-0.7	-2.1	Not shown
4. Cast-mono HIP-MWT	15.6 × 15.6 cm ² , p-type, LFC	36.6	36.9	-0.3	-0.8	Figs. 3 and 6
5. Cz-Si HIP-MWT	15.6 × 15.6 cm ² , p-type	39.5	40.0	-0.5	-1.3	Not shown
6. Fz-Si Honeycomb text, Al-BSF	15.6 × 15.6 cm ² , p-type	35.0	34.9	+0.1	+0.3	Fig. 4
7. Fz-Si IBC	2 × 2 cm ² , n-type	39.2	39.6	-0.4	-1.0	Fig. 5

radiation while the LED spectrum has most intensity in the visible range. From the histograms and J_{SC} maps, we observe that a halogen lamp irradiation (b) would yield a rather homogeneous distribution of poor J_{SC} at the center and rather high J_{SC} around the cell edge due an effect of the cell production described earlier for Fig. 3 Roi C. The situation strongly changes for the LED spectrum (c) because the gain at the cell edge observed for infrared radiation is negligible, while certain grains show over 8% relative drop in J_{SC} due to poor blue spectral response caused by high reflectance. For a given irradiance spectrum, this analysis yields information on which local current extraction properties are critical and which are negligible for optimum solar cell performance.

The average J_{SC} of the cell is 36.1 mA cm⁻² in (a), 30.1 mA cm⁻² in (b) and 39.7 mA cm⁻² in (c). This shows that, relative to the AM1.5G spectrum, this solar cell performs best for the sample LED spectrum and worst for halogen light. This result becomes clear when comparing the photon flux with the average EQE (top), where the LED spectrum follows the EQE more favorably for high J_{SC} than the halogen lamp.

3.5. Impact on other cell parameter imaging methods

In recent years, luminescence imaging (PL/EL) and lock-in thermography (LIT) have been widely established for qualitative and quantitative imaging based characterizations, particularly for industrial silicon solar cells and modules. Prominent quantitative applications of PL are series-resistance imaging [25,26], saturation current density imaging (J_0) [27], as well as imaging of all parameters of the two-diode model [28]. Breitenstein et al. also developed cell parameter imaging of all two-diode model parameters based on dark lock-in thermography images (DLIT) [29].

All of the aforementioned methods operate under the assumption, that J_{SC} is homogenous over the entire active cell area. However, as all J_{SC} maps and particularly the histograms of multicrystalline silicon solar cells in this work have shown, there can be relative differences beyond 20% in J_{SC} . In Fig. 3(b) for example, Roi C has an average J_{SC} of 39.8 mA cm⁻², while Roi B shows only 31.7 mA cm⁻².

Since the spread of J_{SC} across the active cell area is often greater than 10%, we conclude that the homogeneous J_{SC} approximation could significantly influence the results of the aforementioned cell parameter imaging methods. The spatial resolution is also higher than the one usually obtained from PL/EL and lock-in thermography and could even be further increased by appropriate optics. Also, J_{SC} maps could easily be blurred by image processing if necessary. However, the data acquisition time for J_{SC} maps of large industrial solar cells is typically of the order of hours since it increases linearly with sample size. This makes an inclusion of J_{SC} maps by SR-LBIC for in-line cell parameter imaging by luminescence imaging impossible. In the case of PL imaging methods, an SR-LBIC map at the same wavelength as the excitation laser in PL imaging, scaled to match the global J_{SC} , would already be sufficient for such studies. The method proposed in this work delivers the

necessary J_{SC} maps, which was a missing part to be included in the ongoing research about error analysis of these different approaches. Further research is necessary to assess the quantitative impact of the non-homogeneous J_{SC} .

4. Discussion and conclusion

In this work, we demonstrated an easily implementable method of generating short-circuit density maps for arbitrary irradiance spectra using commercially available SR-LBIC instruments by interpolation of local quantum efficiency and integration with the AM1.5G spectrum.

The resulting average J_{SC} match well with those obtained from conventional sun simulator measurements and do not require additional scaling. Table 1 summarizes the absolute values and deviations between averaged J_{SC} from SR-LBIC with those obtained from IV measurements for all solar cells studied in this work.

The deviations of the average values range between +1.8% and -2.1%. There is no clear trend as to whether the linear interpolation over or underestimates J_{SC} because it depends on how well the linear interpolation fits in each case. We would like to reiterate that for non-calibrated sun simulator IV measurements, the measurement error is estimated to be approximately +/- 2%.

The approach presented in this work offers numerous application possibilities for local current loss analysis of arbitrary silicon solar cells with a resolution below 100 μm. The high spatial resolution allows for the study of local quantum efficiencies versus wavelength, which yields information on material quality and local current extraction efficiency. Purely electrical device properties can now be studied more exclusively with a newly introduced Pseudo- J_{SC} map obtained from internal quantum efficiency measurements, which separates electrical and optical losses. All of these results can be obtained from one set of SR-LBIC maps, without compromising on any of the depth-resolved information. In addition, the resulting images are of interest for all established luminescence and lock-in thermography characterization methods that use the assumption of a homogeneous J_{SC} .

Finally, this method has potential for other types of advanced data analysis, specific to the investigated cell structure and material properties. With an appropriate selection of laser wavelengths, the principle of this technique should be applicable to any solar cell structure that allows SR-LBIC measurements, such as thin film, III-V semiconductors and even organic solar cells.

Acknowledgment

The authors would like to thank pv-Tools GmbH for technical support, Elisabeth Schäffer and Stephen Haag for measurements, Karola Rühle for irradiance spectra, Christian Reichel, Philipp Löper and Manuel Schnabel for fruitful discussions as well as the department Solar Cells—Development and Characterization SEC at

Fraunhofer ISE. This work has been partially funded by the German Federal Ministry for the Environment, Nature Conservation and Nuclear Safety under Contract number 0325447 (OHM). Milan Padilla would like to thank the Reiner Lemoine Stiftung for funding his dissertation project.

References

- [1] C. Donolato, Evaluation of diffusion lengths and surface recombination velocities from electron beam induced current scans, *Applied Physics Letters* 43 (1) (1983) 120–122.
- [2] J.D. Zook, Theory of beam-induced currents in semiconductors, *Applied Physics Letters* 42 (7) (1983) 602–604.
- [3] K.L. Luke, O. von Roos, L.-J. Cheng, Quantification of the effects of generation volume, surface recombination velocity, and diffusion length on the electron-beam-induced current and its derivative: determination of diffusion lengths in the low micron and submicron ranges, *Journal of Applied Physics* 57 (6) (1985) 1978–1984.
- [4] W.D. Sawyer, An improved method of light-beam induced current characterization of grain boundaries, *Journal of Applied Physics* 59 (7) (1986) 2361–2363.
- [5] M. Stemmer, S. Martinuzzi, Mapping of local minority carrier diffusion length applied to multicrystalline silicon cells, in: Proceedings of the 11th European Photovoltaic Solar Energy Conference, Montreux, Switzerland, 1992.
- [6] M. Rinio, et al., Defects in the deteriorated border layer of block-cast multicrystalline silicon ingots, in: Proceeding of the 19th European Photovoltaic Solar Energy Conference, Paris, France, 2004.
- [7] W. Warta, et al., Impact of diffusion length distributions on the performance of mc-silicon solar cells, in: Proceedings of the 2nd World Conference on Photovoltaic Energy Conversion, 1998, Vienna, Austria, European Commission, Ispra, Italy, 1998.
- [8] J. Isenberg, O. Bartels, W. Warta, Separation of bulk diffusion length and rear surface recombination velocity in SR-LBIC mappings, in: Proceedings of the 29th IEEE Photovoltaics Specialists Conference, New Orleans, Louisiana, USA, 2002.
- [9] V. Schlosser, et al., LBIC investigations of multicrystalline silicon solar cells with the front contact on grain boundaries, in: Proceedings of the 20th European Photovoltaic Solar Energy Conference, Barcelona, Spain, 2005.
- [10] pv-tools GmbH, Available from: <http://www.pv-tools.de>.
- [11] B. Fischer, Loss analysis of crystalline silicon solar cells using photoconductance and quantum efficiency measurements, *Fachbereich Physik, Universität Konstanz, Konstanz* (2003) 198.
- [12] A.G. Aberle, S. Glunz, W. Warta, Impact of illumination level and oxide parameters on Shockley-Read-Hall recombination at the Si-SiO₂ interface, *Journal of Applied Physics* 71 (9) (1992) 4422–4431.
- [13] M.A. Green, Self-consistent optical parameters of intrinsic silicon at 300 K including temperature coefficients, *Solar Energy Materials and Solar Cells* 92 (11) (2008) 1305–1310.
- [14] B. Thaidigsmann, et al., The path to industrial production of highly efficient metal wrap through silicon solar cells, *Green* 2 (4) (2012) 171–176.
- [15] E. Schneiderlöchner, et al., Laser-fired contacts (LFC), in: Proceedings of the 17th European Photovoltaic Solar Energy Conference, WIP-Munich and ETA-Florence, Germany, 2001.
- [16] H. Hauser, et al., Honeycomb texturing of silicon via nanoimprint lithography for solar cell applications, *IEEE Journal of Photovoltaics* 2 (2) (2012) 114–122.
- [17] K.R. McIntosh, L.P. Johnson, Recombination at textured silicon surfaces passivated with silicon dioxide, *Journal of Applied Physics* 105 (2009) 124520-1–124520-10.
- [18] D. Smith, et al., Generation III high efficiency lower cost technology: transition to full scale manufacturing, in: Proceedings of the 38th IEEE Photovoltaic Specialists Conference, Austin, USA, 2012.
- [19] C. Reichel, et al., Enhanced current collection in backcontacted back-junction Si solar cells by overcompensating a boron emitter with a phosphorus base-type doping, *Physica Status Solidi A* 207 (8) (2010) 1978–1981.
- [20] M. Padilla, et al., Surface recombination parameters of interdigitated-back-contact silicon solar cells obtained by modeling luminescence images, *Solar Energy Materials and Solar Cells* <http://dx.doi.org/10.1016/j.solmat.2013.05.050>, in press.
- [21] Deconvolution plugin developed by the Biomedical Imaging Group—EPFL, Switzerland.
- [22] W.S. Rasband, ImageJ, Available from: <http://imagej.nih.gov/ij/>, 1997–2012.
- [23] N.H. Reich, et al., Crystalline silicon cell performance at low light intensities, *Solar Energy Materials and Solar Cells* 93 (2009) 1471–1481.
- [24] K. Ruhle, S.W. Glunz, M. Kasemann, Towards new design rules for indoor photovoltaic cells, in: Proceedings of the Photovoltaic Specialists Conference (PVSC), 2012 38th IEEE, 2012.
- [25] T. Trupke, et al., Spatially resolved series resistance of silicon solar cells obtained from luminescence imaging, *Applied Physics Letters* 90 (093506) (2007) 1–3.
- [26] J. Haunschild, et al., Fast series resistance imaging for silicon solar cells using electroluminescence, *Physica Status Solidi RRL* 3 (2009) 227–229.
- [27] M. Glatthaar, et al., Spatially resolved determination of the dark saturation current of silicon solar cells from electroluminescence images, *Journal of Applied Physics* (2009) 113110-1–113110-5.
- [28] C. Shen, H. Kampwerth, M. Green, Spatially resolved photoluminescence imaging of essential silicon solar cell parameters, in: Proceedings of the 38th IEEE Photovoltaic Specialists Conference, Austin, USA, 2012.
- [29] O. Breitenstein, Nondestructive local analysis of current-voltage characteristics of solar cells by lock-in thermography, *Solar Energy Materials and Solar Cells* 95 (10) (2011) 2933–2936.